AGU PUBLICATIONS

Water Resources Research

RESEARCH ARTICLE
10.1002/2014WR016150

Integrating multiple scales of hydraulic conductivity measurements in training image-based stochastic models

K. Mahmud[1,2], G. Mariethoz[2,3,4], A. Baker[1], and A. Sharma[2]

[1]Connected Waters Initiative Research Centre, University of New South Wales, Sydney, New South Wales, Australia, [2]School of Civil and Environmental Engineering, University of New South Wales, Sydney, New South Wales, Australia, [3]Institute of Earth Surface Dynamics, University of Lausanne, Lausanne, Switzerland, [4]Department of Earth Sciences, ETH Zurich, Zurich, Switzerland

Key Points:
- Integrating multiple scales of K outside the multi-Gaussian framework
- The use of upscaling to create a multivariate training image
- The application of multivariate Image Quilting

Correspondence to:
G. Mariethoz,
gregoire.mariethoz@minds.ch

Citation:
Mahmud, K., G. Mariethoz, A. Baker, and A. Sharma (2015), Integrating multiple scales of hydraulic conductivity measurements in training image-based stochastic models, *Water Resour. Res.*, *51*, doi:10.1002/2014WR016150.

Received 17 JUL 2014
Accepted 17 DEC 2014
Accepted article online 26 DEC 2014

Abstract Hydraulic conductivity is one of the most critical and at the same time one of the most uncertain parameters in many groundwater models. One problem commonly faced is that the data are usually not collected at the same scale as the discretized elements used in a numerical model. Moreover, it is common that different types of hydraulic conductivity measurements, corresponding to different spatial scales, coexist in a studied domain, which have to be integrated simultaneously. Here we address this issue in the context of Image Quilting, one of the recently developed multiple-point geostatistics methods. Based on a training image that represents fine-scale spatial variability, we use the simplified renormalization upscaling method to obtain a series of upscaled training images that correspond to the different scales at which measurements are available. We then apply Image Quilting with such a multiscale training image to be able to incorporate simultaneously conditioning data at several spatial scales of heterogeneity. The realizations obtained satisfy the conditioning data exactly across all scales, but it can come at the expense of a small approximation in the representation of the physical scale relationships. In order to mitigate this approximation, we iteratively apply a kriging-based correction to the finest scale that ensures local conditioning at the coarsest scales. The method is tested on a series of synthetic examples where it gives good results and shows potential for the integration of different measurement methods in real-case hydrogeological models.

1. Introduction

Numerical simulation of groundwater flow and solute transport is nowadays widely employed to predict available groundwater resources or the fate of pollutant plumes. Hydraulic conductivity (K) defines the ease with which a fluid can move through pore spaces or fractures of a medium, and is the most influential parameter in numerical models.

An important issue in the numerical simulation of groundwater flow and mass transport is the problem of scale dependence of hydraulic conductivity. In a heterogeneous aquifer, preferred pathways and transmissive portions are expected to be encountered when larger volumes of a medium are tested (e.g., when larger-scale tests like pumping tests are compared to permeameter measurements), resulting in an increase of hydraulic conductivity. When comparing measurements from different methods, a consistent increase in K was observed or proposed by various authors [*Clauser*, 1992; *Herzog and Morse*, 1986; *Neuman*, 1990; *Rovey and Cherkauer*, 1995; *Schulze-Makuch and Cherkauer*, 1998]. Either the volume of rock tested or the radius of influence of an aquifer test is commonly the measure used to examine the scale dependence of K. *Schulze-Makuch and Cherkauer* [1998] analyzed conductivity measurements made with different methods in a given geological formation. They showed that the increase in hydraulic conductivity with scale of measurement occurs up to the position of an upper bound, after which the medium behaves as a homogeneous medium and K remains constant with scale. Further, it has been argued that a value of hydraulic conductivity is necessarily associated to a support volume, and that no punctual estimation can be given for it [*Emsellem and De Marsily*, 1971; *Matheron*, 1967].

Given this nonlinear scale dependence of hydraulic conductivity, it can be challenging to simultaneously take into account hydraulic conductivity measurements taken at different scales. This paper focuses on the question of simultaneous integration of hydraulic conductivity data representing different investigated

volumes, in the context of training image-based stochastic models where the strong heterogeneity makes the relationships between scales complicated.

Dagan [1986] discusses three support scales: the laboratory, the local, and the regional scale. In terms of data, information is usually collected at scales that are different than the elements used in numerical models. In practical applications, K measurements are taken using slug tests, well tests, lab measurements, or even indirectly with airborne remote sensing measurements [*Dickson et al*., 2014; *Koch et al*., 2014]. All these measurements need to be "translated" into the scale of the model. In the context of multi-Gaussian models, analytical formulations are available that can estimate equivalent hydraulic conductivity as a function of spatial parameters and scale [*Dagan*, 1989; *Emery*, 2008; *Renard and De Marsily*, 1997]. These are based on the assumption that the scale dependence of permeability follows a geometric average [*Matheron*, 1967], thus offering a convenient way to translate hydraulic conductivity values across scales. *Tran* [1996] proposed an approach in the framework of a multi-Gaussian model, consisting in establishing an empirical relation between the small scale and the block scale by using a numerical upscaling method, and then calibrating a two-scale geostatistical model. It gave rise to interesting studies in the field of inverse problems resolution using multiple scales of models [*Gardet et al*., 2014]. However, those methods do not hold when the medium is not multi-Gaussian or presents strong heterogeneities. This is especially problematic when using geostatistical methods focused on strongly heterogeneous media, such as Multiple-Point Simulation (MPS), object-based or pluri-Gaussian models. In this paper, we propose an approach that builds on the work of *Tran* [1996] and generalizes it to nonmulti Gaussian models.

Scale translation can go in two directions: it can be either upscaling (from a small scale to a coarser scale) or downscaling (from a coarse scale to a smaller scale). In the first case, one has to estimate a single equivalent parameter for a group of smaller model elements where measurements exist. In the second case, the small-scale variability of a given area must be reconstituted under the constraint that the equivalent parameter for this area corresponds to a large-scale measurement.

The question of upscaling has been thoroughly studied in the last decades. Upscaling is needed when a detailed geological description allows representing small-scale spatial features. Complex geological models are routinely built; however, these models require fine discretization and are computationally prohibitive when directly used for flow simulation, particularly in the context of sensitivity studies, inverse modeling, or Monte-Carlo analyses, which require multiple runs of the computer codes. While computational power has significantly increased in the last years, the maximum discretization that can be realistically simulated is still limited to few million cells. Using upscaling to transform hydraulic conductivities from the scale of the geological model to the coarser scale of the flow model has been the subject of research for many years [*Botros et al*., 2006; *Emery*, 2009; *Gomez-Hernandez and Gorelick*, 1989; *Renard and De Marsily*, 1997; *Sanchez-Vila et al*., 2006; *Zhou et al*., 2010].

Another use of upscaling arises when data are available at a smaller scale than the model elements. This can be the case in mining studies, where drill holes provide mineral grades on a much smaller support size than the mining blocks where mineral concentrations have to be estimated. Block simulation has been extensively used in such mining applications [*Boucher and Dimitrakopoulos*, 2012; *Deutsch*, 2006; *Emery and Ortiz*, 2011; *Gomez-Hernandez and Journel*, 1994; *Marcotte*, 1994]. However, these methods are not applicable for hydraulic conductivity which is not an additive variable: as mentioned above, it is not possible to calculate an equivalent permeability by a simple arithmetic mean.

The downscaling problem is more difficult because large-scale measurements do not uniquely inform the small scale. It then becomes necessary to use stochastic approaches that construct multiple small-scale models having spatial characteristics compatible with the sedimentary processes that led to the creation of the reservoir rocks [*Koltermann and Gorelick*, 1992; *Tang et al*., 2013a]. This is however difficult because such process-based models cannot be easily constrained to local data or regional averages. Methods have been designed for geostatistical simulation with block constraints on a large scale [*Kupfersberger et al*., 1998; *Liu and Journel*, 2009; *Ren et al*., 2008], which could be used to populate small-scale hydraulic conductivity conditioned to large-scale measurements (e.g., well test data). However, these methods are also limited to media presenting a low degree of heterogeneity and simple connectivity patterns, and therefore are only applicable in conjunction with variogram-based spatial models.

In this paper, we present a solution for simultaneously assimilating hydraulic conductivity data at different scales (upscaling as well as downscaling) without invoking multi-Gaussian assumptions, and we test the

method on synthetic example cases. Its principle is to start from a training image that describes a geologically realistic variability for the domain considered at the smallest measured scale (e.g., core scale). Such a training image could be obtained, for example, from a process-based model that produces physically realistic small-scale properties [*McHargue et al.*, 2011]. Then, using classical upscaling approaches such as the ones described above, this training image is coarsened to larger scales corresponding to other types of measurements (e.g., slug tests, well tests). This results in a multivariate training image that describes physically correct interscale relationships for the type of heterogeneity considered. A multivariate simulation algorithm is then used to create multiscale models that are conditioned to all measurements simultaneously, for all scales considered.

The methodology presented here uses Image Quilting [*Mahmud et al.*, 2014] as a multivariate MPS algorithm, and Simplified Renormalization [*Renard et al.*, 2000] as an upscaling technique, but our workflow is general and these algorithms could in principle be substituted by any other combination of a multiple-point simulation and a numerical upscaling algorithm. The novelty of our approach is to put together these different elements in a multiscale workflow for integrating data at different scales. In addition, we present the first implementation and application of multivariate MPS in the context of patch-based methods.

2. Methodology

2.1. Background on Image Quilting (IQ)

Guardiano and Srivastava [1993] suggested the first multiple-point geostatistics (MPS) approach based on the assessment of the conditional probability distribution for a simulated value based on a training image (TI). The term multiple-point statistics is used in reference to the traditional variogram model used with kriging that only takes into consideration the average square difference between two points, i.e., a measure of two-point statistics. The variogram characterizes spatial patterns between pairs of points and often fails to capture important geological patterns such as connectivity and curvilinearity. MPS simulation aims at characterizing patterns using several points, typically between 15 and 80, instead of two, thus providing a more realistic representation of geological patterns [*Mariethoz and Caers*, 2014]. There are now many MPS algorithms available, e.g., SNESIM [*Strebelle*, 2002], SIMPAT [*Arpat and Caers*, 2007], FILTERSIM [*Wu et al.*, 2008; *Zhang et al.*, 2006], IMPALA [*Straubhaar et al.*, 2011], HOSIM [*Mustapha and Dimitrakopoulos*, 2011], MCP [*Allard et al.*, 2011], MPPCA [*Abdollahifard and Faez*, 2013], CCSIM [*Tahmasebi et al.*, 2012], Direct Sampling [*Rezaee et al.*, 2013], Image Quilting [*Mahmud et al.*, 2014] that are currently being used in real-world applications. TIs used in MPS methods may originate from real data representative of the geology under consideration [*Jung et al.*, 2013], outcrops [*Falivene et al.*, 2006], remote sensing data [*Tang et al.*, 2013b], large unconditional realizations of another stochastic simulation technique [*Comunian et al.*, 2014], or be based on sketches produced by geologists [*Natali et al.*, 2014]. The concept of simulating models using Multiple-Point statistics from a TI seems easy, straightforward, and smart for geologists [*Hu and Chugunova*, 2008]. From its original applications in reservoir modeling [e.g., *Caers et al.*, 2003; *Huysmans and Dassargues*, 2012; *Ronayne et al.*, 2008], MPS algorithms have been used for a broad spectrum of applications relevant to water resources modeling, such as remote sensing [*Boucher et al.*, 2008; *Gibson*, 1950; *He et al.*, 2013; *Mariethoz et al.*, 2012], climate modeling [*Jha et al.*, 2013; *Oriani et al.*, 2014], physics of fluids in porous media [*Farmer*, 2002; *Hajizadeh et al.*, 2011; *Okabe and Blunt*, 2007; *Tahmasebi and Sahimi*, 2013], and even medical imaging [*Pham*, 2012; *Tsunoyama et al.*, 2014].

A recent review [*Mariethoz and Lefebvre*, 2014] showed that the field of computer graphics, and in particular, texture synthesis methods, pursues goals similar as MPS: to generate images made of similar patterns as a training image (or exemplar), and showing stochasticity (i.e., are not a repetitive tiling of the same patterns). Originating from texture synthesis, the method of Image Quilting was initially proposed by *Efros and Freeman* [2001] and considers blocks or patches rather than taking a particular pixel as the simulation unit. This is similar as patch-based geostatistical methods [*Arpat and Caers*, 2007; *El Ouassini et al.*, 2008; *Faucher et al.*, 2012; *Tahmasebi et al.*, 2012; *Zhang et al.*, 2006].

Whereas many geostatistical patch-based methods use patterns databases to store and search patterns, IQ is part of a family of MPS algorithms that directly search patterns in the training image, which notably includes CCSIM [*Tahmasebi et al.*, 2012]. For each neighborhood N, a separate convolution is performed, denoted $C(\mathbf{y}) = TI(\mathbf{y}) * N$, where $\mathbf{y}$ is a location in the training image and the symbol * denotes a convolution operation. Any norm can be used for the convolution, whether the variable is continuous or categorical. For

example, CCSIM involves computing a convolution based on a cross-correlation function, which provides increased computational efficiency. In IQ, *Mahmud et al*. [2014] do not use a cross-correlation function, but rather perform convolutions based on a Euclidean distance for continuous variables, and a distance based on the number of mismatching nodes for categorical variables. The locations with a small convolution value correspond to candidate patches that can be used in the simulation. A specificity of IQ is that once a candidate patch has been sampled, the patch shape is modified by cutting it such that the overlap error is minimized. This minimum error boundary cut was the main contribution of the original method by *Efros and Freeman* [2001]. It consists in using dynamic programming [*Dijkstra*, 1959] to cut the patches such that overlapping artifacts do not appear. A contribution of *Mahmud et al*. [2014] was to further develop the cutting method to adapt it to the 3-D case. The most important parameters in IQ are the patch size p, the overlap size o and the number ε of replicates considered.

Mahmud et al. [2014] present an implementation of IQ that is amenable to be used for subsurface modeling. Compared to the original version of *Efros and Freeman* [2001], important additions are the extension to 3-D models and the possibility to consider conditioning data. For conditioning, the TI is searched for blocks that agree both with their neighbors along the section of overlaps and at the same time all hard data available within the block. Therefore, instead of selecting candidate patches solely based on their overlap with previously simulated areas, the compatibility with conditioning data is also considered. In the case of a continuous variable, it is not possible to condition exactly due to the finite size of the TI (and hence a limited pattern set). In order to have exact conditioning, the iterative template splitting (TS) has been introduced [*Tahmasebi et al*., 2012]. The main idea is that it is easier to honor the hard data with a smaller template size. This is particularly the case when several conditioning data points from different scales fall in a single template, and when the pattern formed by these data has no equivalent in the TIs. In cases where there is no suitable block that exactly matches the data, the template splits in 4 (in 2-D) or 8 (in 3-D). The resulting smaller templates will each contain less data, and therefore will be easier to condition. The operation is carried out recursively, until the template is small enough for conditioning to be feasible.

2.2. Multivariate Image Quilting (MIQ)

Many hydrogeological applications involve the simulation of several variables simultaneously on the same spatial domain. Sometimes the relationship between variables can be modeled with a simple parametric (linear) function, but such is often not the case, for example, for the scale dependence of hydraulic conductivity. For complex dependences, one can use multivariate TIs to convey such relationships. The multivariate TI consists of a set of collocated variables each representing the spatial structure being modeled within that variable, and at the same time representing physically realistic spatial relationships between all the variables. Once such a TI is available, it can be used to generate multivariate spatial patterns that reproduce the desired multivariate relationship. It is noted that the concept of multivariate training images is different from the use of auxiliary variables, which are exhaustively known and typically used to impose nonstationarity [*Chugunova and Hu*, 2008; *Strebelle*, 2002].

In this paper, we are using the joint simulation of variables for multiscale modeling. We consider that the hydraulic conductivity at each scale is a separate variable, and therefore there are as many variables as scales considered. The different scales are not independent, but present complex scale dependencies, which are described by a multivariate TI. A physics-based upscaling method is used to generate such a multivariate TI that has physically consistent scale dependencies. To apply such a multiscale methodology, a necessary preliminary step is to extend the IQ method described above in order to be able to use multivariate training images.

The general concept used in multivariate IQ simulation is very different from that used in the context of variogram-based geostatistics for cosimulations. In this typical framework (cokriging or cosimulation), two or more variables are simulated together by maintaining a given linear model of coregionalization (cross variogram) between the variables. To statistically infer the parameters of multivariate relationships, the only data available are sparse locations where variables are observed simultaneously. In practice however, when multiple hydraulic measurements are available, they are seldom collocated, making it difficult to infer a parametric multivariate model. One scale may be sampled at some locations, while another scale is sampled at different locations. In some areas, information at several scales may overlap. For example, some data at the scales of the core samples (cm) and also at the scale of the well tests (100 m) are known, but no data is available at a larger scale (km).

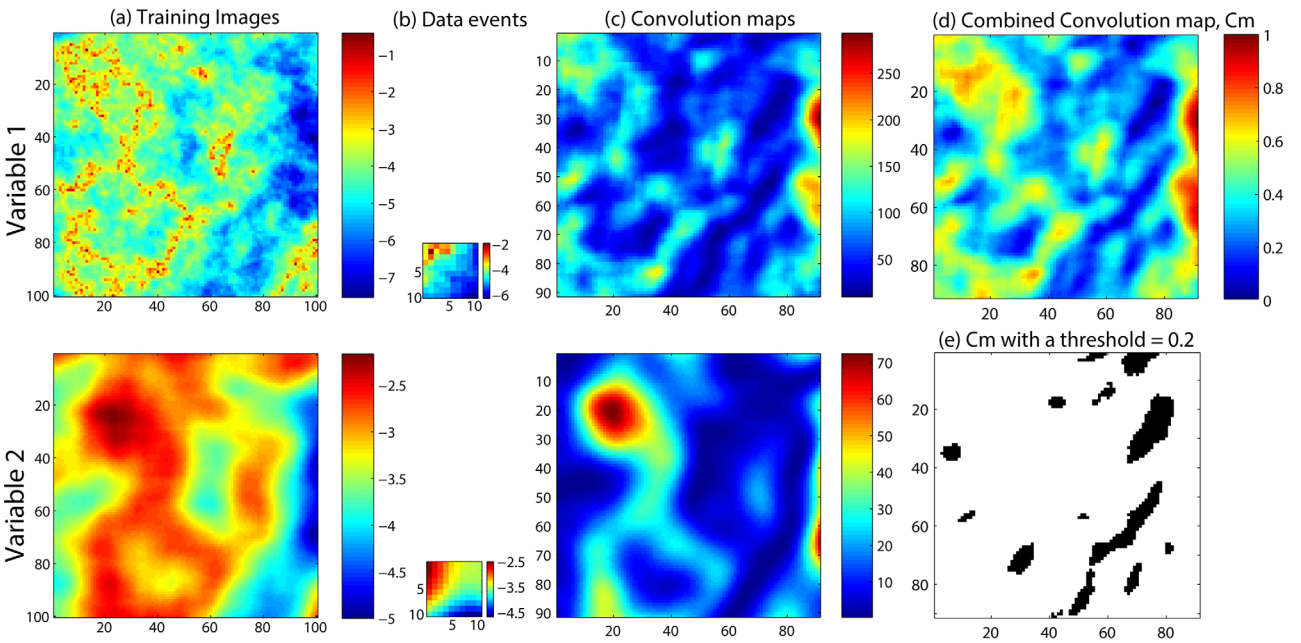

Figure 1. Multivariate convolution showing the thresholded convolution map. (a) Bivariate training image. (b) Bivariate neighborhood. (c) Convolution maps for both variables. (d) Combined convolution is obtained by lumping the individual univariate convolution maps with equal weights. (e) Locations with patterns being similar to the multivariate neighborhood in Figure 1b. The *x* and *y* axis show the grid sizes in all figures, in units of number of grid cells. The color scales for Figures 1a and 1b represent logarithmic hydraulic conductivity values, for Figure 1c, they represent sums of square differences, and for Figure 1d, it indicates the values of $\boldsymbol{C_m}$, normalized in [0 1].

From an algorithmic point of view, the multivariate version of the IQ method follows the same principle as in the univariate case; the difference lies in the use of multivariate neighborhoods and multivariate distances to perform convolutions. Here we provide a simple illustrative example on a synthetic case involving a multivariate convolution, based on the bivariate TI shown in Figure 1. Two variables are considered, consisting of simplified representations of hydraulic conductivity at two different scales. The grid size is 100 × 100 pixels in 2-D. Variable 1 is obtained by the method of *Zinn and Harvey* [2003] that consists in taking the absolute value of a realization sampled from a multi-Gaussian model with zero mean and an isotropic exponential variogram. The realization obtained has an asymmetric histogram. A histogram transformation (normal-score transform) is then used to restore the standard Gaussian histogram. The resulting patterns are complex and difficult to describe with covariance models. One such realization is shown in Figure 1a (top). Note that the values are inversed in this figure such that high values are connected instead of the low values. Variable 2 is defined as a smoothing of variable 1 with a moving average using a window of 17 by 17 pixels, shown in Figure 1a (bottom). The smoothed variable resulting from the moving average operation can be assimilated for example to hydraulic conductivity considered on a larger support size, in a similar fashion as an upscaling operation that coarsens up the detailed spatial features.

Two small blocks randomly taken from another similar bivariate TI are shown in Figure 1b, representing multivariate data events. These blocks have a similar spatial correlation as the TI. The convolution for each variable is obtained independently (Figure 1c) and then normalized in the interval [0 1]. A single multivariate convolution map (Figure 1d) is then obtained by lumping the individual univariate convolutions. The resulting lumped convolution C_m can then be used as a basis for determining the training image locations where the patterns are similar to a given multivariate neighborhood. In the case of *v* variables $G_1 \ldots G_v$, such a lumped convolution is formulated:

$$C_m(\mathbf{y}) = \sum_{G=0}^{v} w_G [TI_G(\mathbf{y}) * N_G]^2 \quad (1)$$

with TI_G being the training image for variable *G*, N_G is the neighborhood considered for variable *G*, and $w_1 \ldots w_v$ are weights given to each variable, summing to 1. Applying a threshold on this error map yields the set of matching locations (Figure 1e), where training image patterns correspond to a given multivariate neighborhood. A location is sampled from this set and the corresponding entire multivariate patch $N = [N_1$

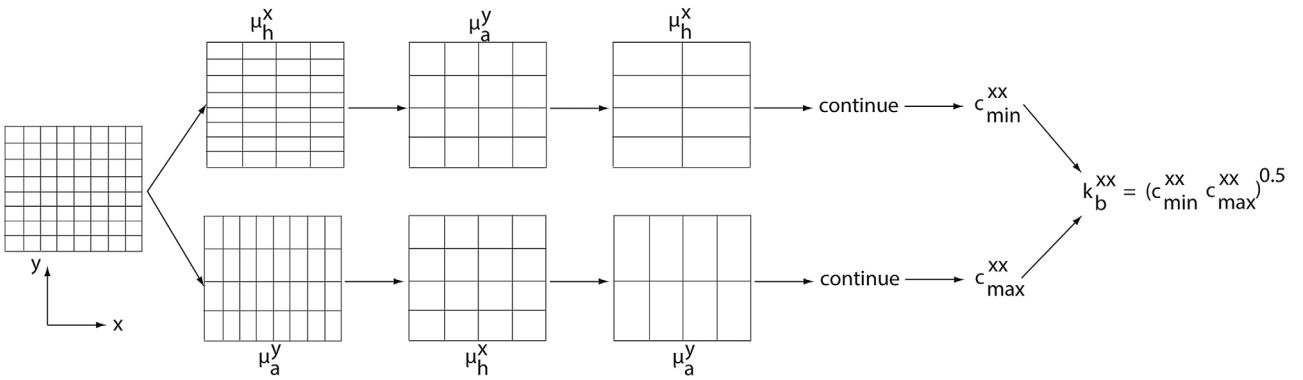

Figure 2. Simplified renormalization procedure in two dimensions. The cells are grouped two by two iteratively in order to finally obtain two values denoted c_{min} and c_{max} and eventually k_b (modified from *Renard et al.* [2000]).

$N_2 \ldots N_v$] is pasted from the training image to the simulation. To define the optimal cut between the patches in the overlapping regions, we compute separately the cumulative minimum errors along the cutting direction as described in *Mahmud et al.* [2014] for all variables. Then we add those errors with the given variable weights to get a single lumped error map. The resulting lumped error map can then be used as the basis for determining a single optimum cut through all different variables. In this way, we can preserve the same complex relationship between the variables as given by the TIs.

2.3. Simplified Renormalization

Among various possible upscaling methods, we applied the technique of *Renard et al.* [2000], which is a recursive algorithm used for fast upscaling. The equivalent permeability of a fine-mesh grid is determined by a series of successive aggregations where meshes are grouped two by two. In a first step, the cells are grouped alternatively in parallel and in series with respect to the direction of calculation. The basic operation is the approximate calculation of equivalent permeability of a cell with 2-D meshes. The *Cardwell and Parsons* [1945] bounds are used to iteratively aggregate groups of cells at the local scale to produce "composite" cells and then to successively reapply the same rules to the resulting composite cells until the desired coarse-scale resolution is achieved. If the two cells are in series (aligned in the direction of the flow lines), they are replaced by a unique cell whose conductivity is the harmonic mean of the conductivity of the cells (μ^x_h, μ^y_h in *x* and *y* directions, respectively). If the two cells are in parallel (placed perpendicularly to the flow lines), the arithmetic mean (μ^x_a, μ^y_b in *x* and *y* direction, respectively) is used. This basic procedure is repeated until a grid of the desired size is obtained, ultimately one single element. In two dimensions (Figure 2), one can start with a grouping in series along the *x* direction, followed by grouping the new pairs in parallel along the y direction, then repeat this basic algorithm until one gets a value that is denoted c^{xx}_{min}:

$$c^{xx}_{min} = \mu^y_a(\ldots\mu^y_a(\mu^x_h)\ldots) \tag{2}$$

Alternatively, one can start with a grouping in parallel along the *y* direction, followed by grouping the new pairs in series along the *x* direction, then one repeat the algorithm to get a value denoted by c^{xx}_{max}:

$$c^{xx}_{max} = \mu^x_h(\ldots\mu^x_h(\mu^y_a)\ldots) \tag{3}$$

The renormalization results in a tensor of upscaled hydraulic conductivities. In our case, we assume that K is isotropic, because we are interested in integrating measurements of hydraulic conductivity such as pumping tests, which generally do not provide a tensor but an isotropic value. We therefore take the norm of the upscaled hydraulic conductivity value:

$$k^{xx}_b = \log_{10}\sqrt{{c^{xx}_{min}}^2 + {c^{xx}_{max}}^2} \tag{4}$$

2.4. Multiscale Modeling With MIQ

Before describing the methodology, we define a set of notations that will be followed throughout the paper:

x designates a location in the simulation and **y** designates a location in the TI;

$G = G_1 \ldots G_v$ the grid level, from finer to coarser;

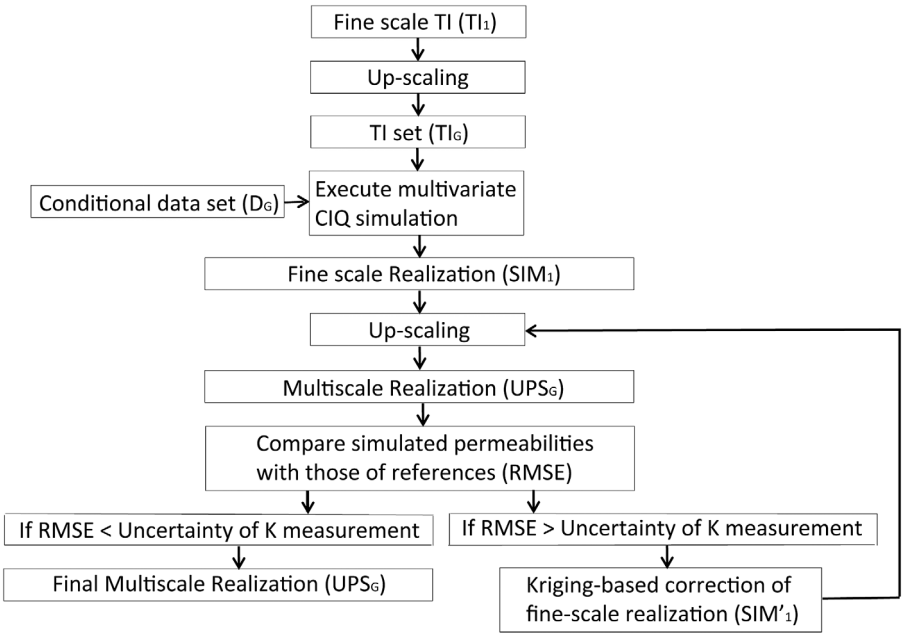

Figure 3. Multiscale data assimilation workflow with Kriging correction.

TI_G the different scales of the training images;

SIM_G the different scales of the MIQ simulation;

UPS_G, with $G = G_2 \ldots G_v$ the upscaled models obtained from SIM_1;

D_G The data available at scale G;

SIM_G' The simulation corrected by kriging.

The key principle of our methodology is to consider different scales of hydraulic conductivity as joint variables, which are simulated together. The complete algorithm is given in Figure 3. Two inputs are provided:

1. Conditioning data, D_G which are hydraulic conductivity measurements having different support sizes (for example, fine-scale hydraulic conductivity from lab tests, coarse scale hydraulic conductivity from in situ pumping tests, etc.).

2. A training image, TI_1 representing hydraulic conductivity at the smallest measured scale.

Based on TI_1 which represents the smallest scale, we use renormalization to obtain a series of upscaled training images, TI_G for scales $G_2 \ldots G_v$ that correspond to the different scales at which measurements are available. Considered together, these upscaled maps constitute a multiscale representation of the hydraulic conductivity.

With these training images TI_G, MIQ is used to obtain a multiscale realization SIM_G that is conditional to the data available, D_G. Each conditioning data point is assigned only to the variable that corresponds to its measurement support. However, the simulation SIM_G is constrained by the multivariate patterns specified in the training image, TI_G. Therefore, conditioning data at one scale can influence the hydraulic values at the other scales, if such dependence is present in the training image. For example, a well test might result in a large hydraulic conductivity value imposed at the coarsest scale. Since the different scales in the training image are obtained with a physically consistent process (the renormalization upscaling), the locations of the TI where high values occur should also present high values at the smaller scales.

At this stage, the result of MIQ is a realization that honors the conditioning data exactly and reproduces the statistical relationships between scales present in the training image. However, this is not sufficient because the scale dependence has a physical basis that is only approximated through the MIQ simulation. As is the case with all multiple-point simulation methods, the training image has a finite size and the statistics it represents might not be reproduced exactly. Moreover, the results of multiple-point simulation are dependent on the implementation and on the parameterization of the simulation algorithm. As a result, it is possible that the relationships

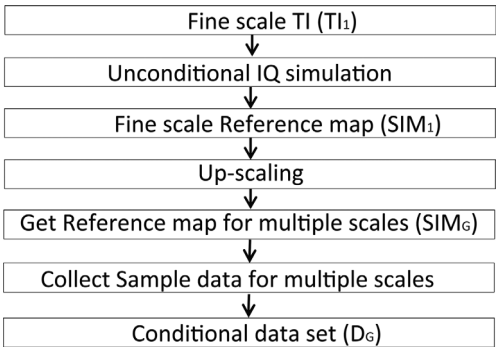

Figure 4. Workflow for the creation of the synthetic reference data set.

between the simulated scales are not physically consistent (even though they are statistically consistent). The scale relationships of the simulated model, SIM_G can however be simply tested: it suffices to take the smallest scale of the realization, SIM_1 (which is conditioned to the fine-scale conditioning data) and apply renormalization upscaling to it. If the result of this upscaling UPS_G honors the coarse-scale conditioning data D_G, for $G_2 \ldots G_v$, then the scale relationships are physically consistent, according to the upscaling method used.

The next step of our methodology consists precisely in performing this test: if, when upscaling is applied, the coarse conditioning data are all honored (or within a given measurement error), then the multiscale model obtained by IQ and renormalization (UPS_G) is physically correct at all scales and consistent with the data D_G, and nothing else needs to be done.

However, if there is a significant mismatch with the coarse data, corrective measures have to be taken. This correction is applied on the finer scale only, because all other scales can be deduced from it using renormalization upscaling. The goal is to perturb the fine-scale hydraulic conductivity SIM_1 such that, when upscaled, the coarse-scale measurements UPS_G for $G_2 \ldots G_v$ are matched. Furthermore, this perturbation should preserve the conditioning data D_1, which are honored at the finest scale. The only way to accomplish this is to add smooth and large-scale perturbations to the small scale, which will have as a consequence to shift the upscaled values up or down. This is done by using kriging, which has the desired properties since it is a smooth interpolator and can be constrained at conditioning locations. Kriging-based corrections are applied iteratively to the small-scale hydraulic conductivity, SIM_1, until the error between the upscaled SIM_G' and the measured coarse data, D_G for $G_2 \ldots G_v$ is small enough (i.e., under the measurement uncertainty).

For this, we initially calculate the errors between the different scales of the simulation UPS_G and the given conditioning data D_G for scales $G_2 \ldots G_v$. Then simple kriging is applied to the fine-scale simulation only, in order to find a correction that minimizes these errors on the scales $G_2 \ldots G_v$ while not affecting the conditioning of grid 1 (which does not need upscaling to achieve conditioning to the data of scale 1). We denote $t(\mathbf{x})$ the kriging-based correction. It is set to zero at all conditioning locations on G_1 (these do not need correction). At the location of data corresponding to the scales $G_2 \ldots G_v$, the correction $t(\mathbf{x})$ is defined as the error between the conditioning data D_G and UPS_G:

$$t(\mathbf{x}) = \sum_{j=1}^{n} \lambda_j Err_j \tag{5}$$

where λ is the kriging weight, n is the total number of data points, and Err is the data mismatch for each data point. Kriging interpolates this error smoothly, which is then subtracted to the fine-scale realization (SIM_1) to correct it:

$$SIM_1' = SIM_1 - t(\mathbf{x}) \tag{6}$$

This minimizes the differences between the new SIM_1' and the data D_G for scales $G_2 \ldots G_v$, while leaving it unaffected at the locations of the fine-scale data D_1. Then we perform another test by upscaling the SIM_1' and if there are remaining conditioning errors we repeat kriging corrections until all conditioning data points are exactly satisfied at all scales. Each iteration will necessarily reduce the difference between measured and modeled values. We found that in practice all hydraulic conductivity values at all scales are reproduced after a relatively small number of kriging iterations (no more than three iterations in the test cases considered).

We emphasize that the kriging correction is only applied to the fine-scale hydraulic conductivity map G_1, but it results in affecting the other scales when G_1 is upscaled. The smooth corrections around the data points ensure that the heterogeneity patterns are not significantly affected. One limitation is that if the kriging-based correction becomes too strong, it may affect the structures simulated with MIQ, resulting in a change in the connectivity properties of the simulation. Therefore, when using this method one should quantify the amount of kriging

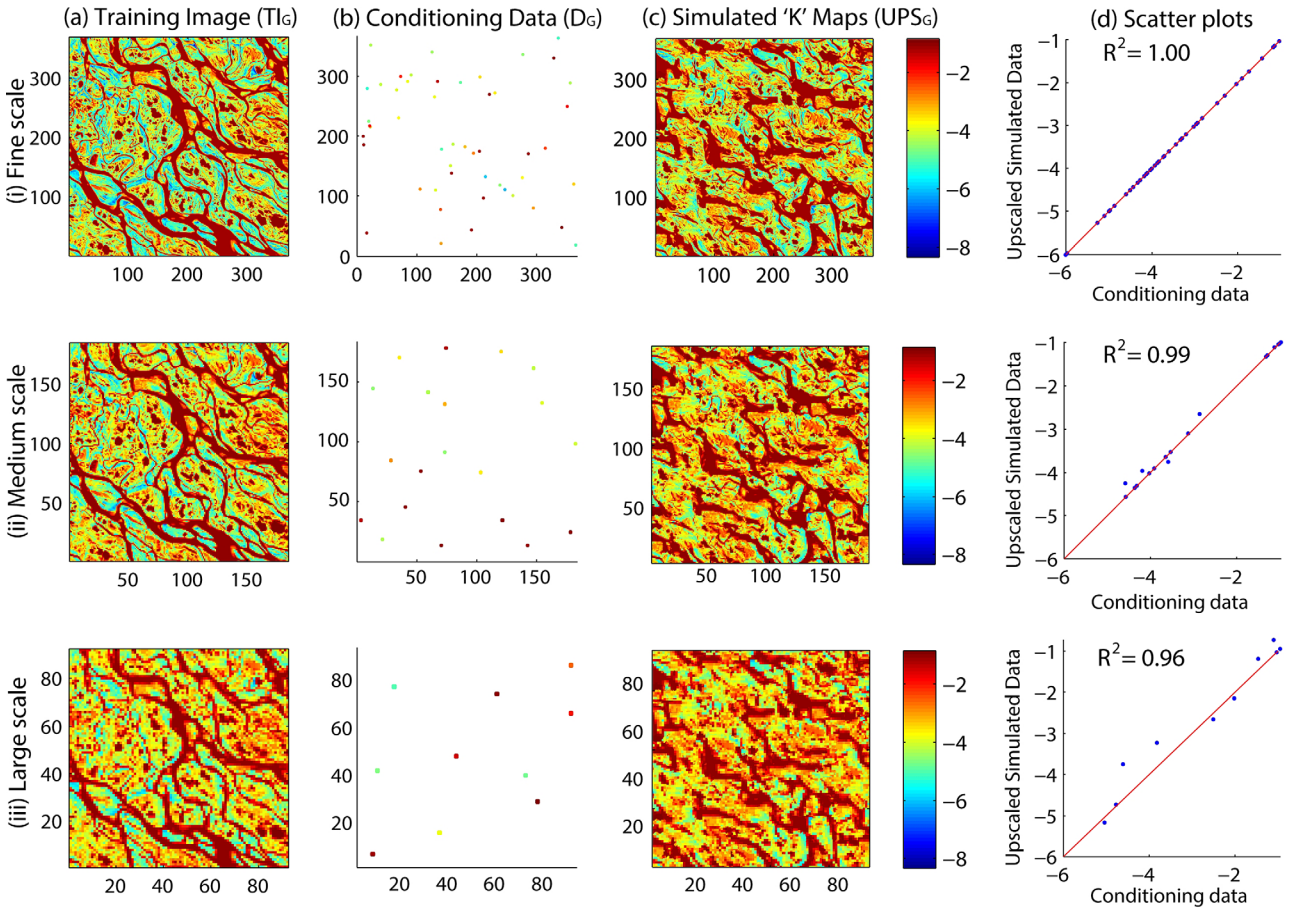

Figure 5. Performance of data conditioning with MIQ for a continuous field with three different scales. The same colorbar is used for TI, Conditioning data, and Simulated K maps, which represent the logarithm of hydraulic conductivity. The *x* and *y* axis show the number of grid cells.

correction and use the results carefully if very large corrections have been used to achieve conditioning. This is investigated in detail in the case studies section.

3. Application Examples

3.1. Test Case 1: Highly Connected Features

We consider a first synthetic case with three scales and three corresponding data sets. We have chosen to work with synthetic examples in this paper because they allow validating the results against a known reference. Moreover, a real case might have additional sources of uncertainty such as the choice of the TI. Here we only want to evaluate our multiscale data integration method, for which synthetic examples provide controlled conditions.

To create the conditioning data sets, we follow the algorithm shown in Figure 4. This case study uses the fine scale TI (TI_1) shown in Figure 5a (top), representing the logarithm of hydraulic conductivity values generated from a Landsat 7 image of the Lena Delta in Russia. It is used to represent synthetic hydraulic conductivity. The channels are highly connected and therefore can create complex relationships between scales. We use the renormalization upscaling technique to obtain the corresponding hydraulic conductivity at two coarser scales shown in Figure 5a (middle and bottom). This multivariate TI is used with conditioning data (Figure 5b) taken randomly from an unconditional multiscale realization simulated by IQ. Different random conditioning locations are chosen at each scale. We sample 50, 20, and 10 data points for fine, medium and coarse scales, respectively. The sizes of both the TIs and simulation grids (SGs) are 368 × 368 fine-scale pixels. MIQ simulation is used to obtain the fine-scale hydraulic conductivity realization, with parameters as

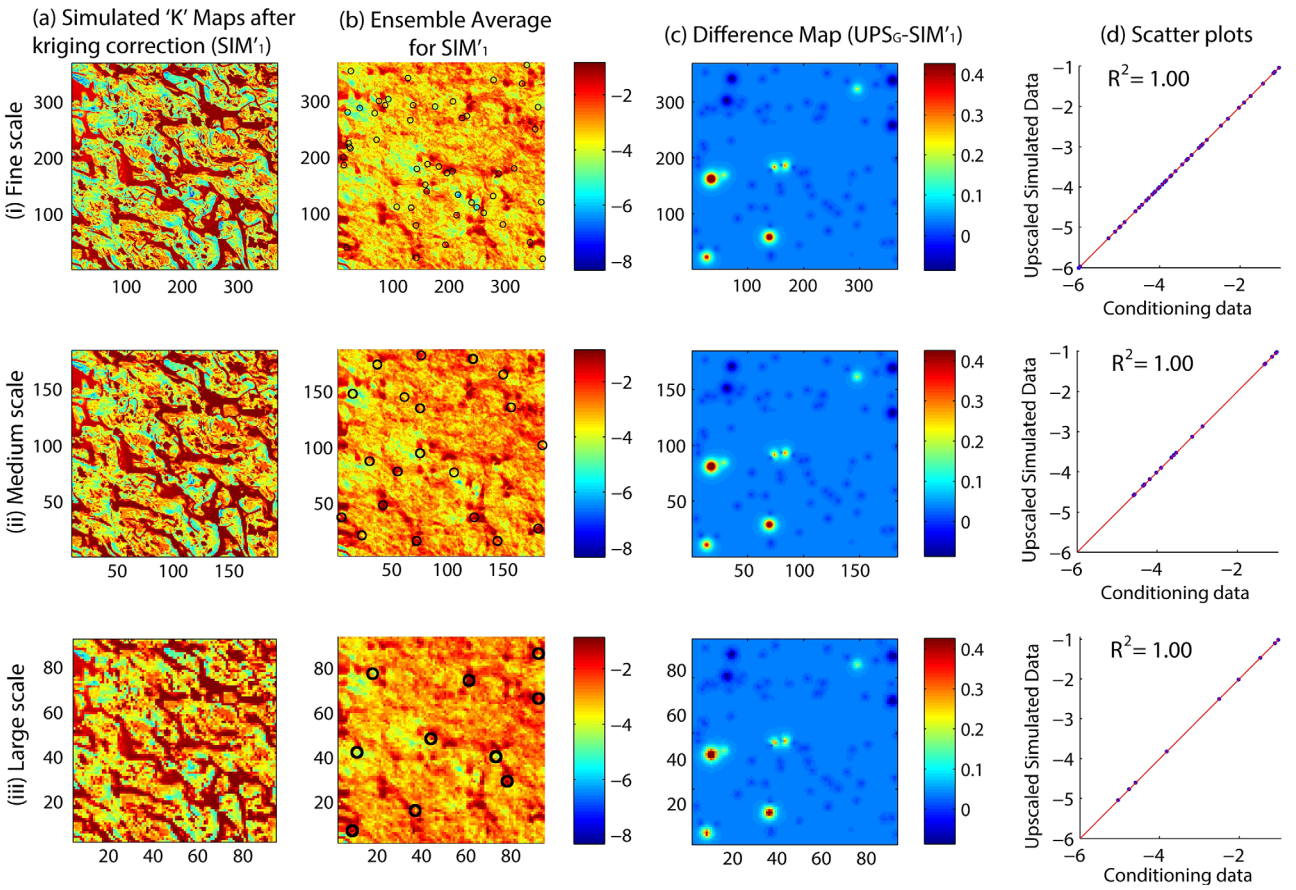

Figure 6. Performance of data conditioning using upscaling with kriging correction. The same colorbar is used for Simulated K maps and ensemble averages, which represent logarithm of hydraulic conductivity values. The *x* and *y* axis show the number of grid cells. Data locations are shown in ensemble averages with black circles.

follows: patch size $p = 30 \times 30$ pixels, an overlap region of $o = 8$ pixels and $\varepsilon = 10$ replicates. These parameters have been shown to provide good results according to the sensitivity analysis carried out in *Mahmud et al*. [2014].

Having set out the synthetic case, we execute the algorithm shown in Figure 3. One fine-scale realization is shown in Figure 5c (top). We then use renormalization upscaling to produce large-scale conductivity maps based on the fine-scale realization. Upscaled conductivity maps are shown in Figure 5c (middle and bottom). The fine-scale simulation obtained by MIQ naturally honors all fine-scale data points, but for larger scales the conditioning is not exact. Conditioning data match is shown as scatter plots in Figure 5 with the R^2 values indicated. The next section will show how a kriging-based correction can be used to make sure that all conditioning data points are honored.

Our goal is that the realizations correspond to the measured values for all different scales (or exhibit a mismatch reflective of the measurement error). To this end, we follow the algorithm described in section 2.4 and perform iterative kriging corrections of all the error values calculated for larger scales, until all data points, at all scales, are satisfied within a given RMSE. The variogram model used for kriging has the following parameters: range = 15, sill = 2.115, and nugget = 0.45, which are inferred from the fine-scale training image. The target RMSE is set to 10^{-5}, which was obtained after two iterations taking 96 s. Figure 6a shows the simulated hydraulic conductivity maps after iterative kriging corrections have been applied, as well as ensemble averages of 20 conditional realizations (Figure 6b). The difference maps shown in Figure 6c quantify the effect of the kriging correction on the simulated hydraulic conductivity maps, showing that its magnitude is small compared to the range of simulated values. The cross plots (Figure 6d) and the R^2 values illustrate that our method allows exact conditioning of all data points for different scales.

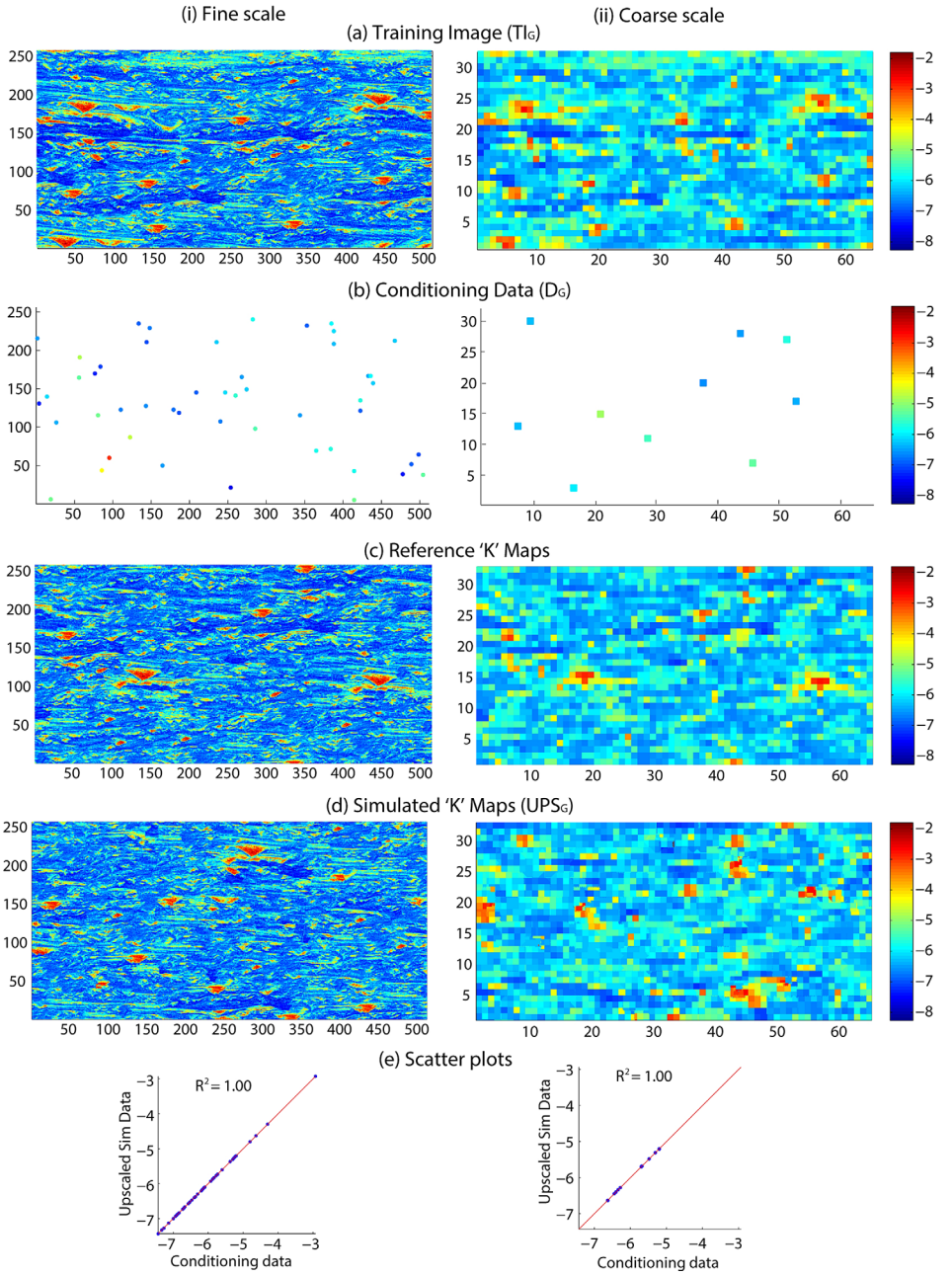

Figure 7. Univariate IQ simulation for a continuous TI with two different scales. (a) Multiscale training image. (b) Conditioning data randomly sampled from (c) the reference model. (d) Models conditioned to each scale independently. (e) Conditioning accuracy when modeling each scale independently.

3.2. Test Case 2: Large Upscaling Factor

3.2.1. Univariate IQ Simulation

We consider another synthetic case with 2 variables and create the conditioning data sets and the reference maps by following again the algorithm shown in Figure 4. Specifically, this test case consists of the following steps:

1. Define the training image.

2. Use it to generate the reference hydraulic conductivity fields.

3. Sample conditioning data sets.

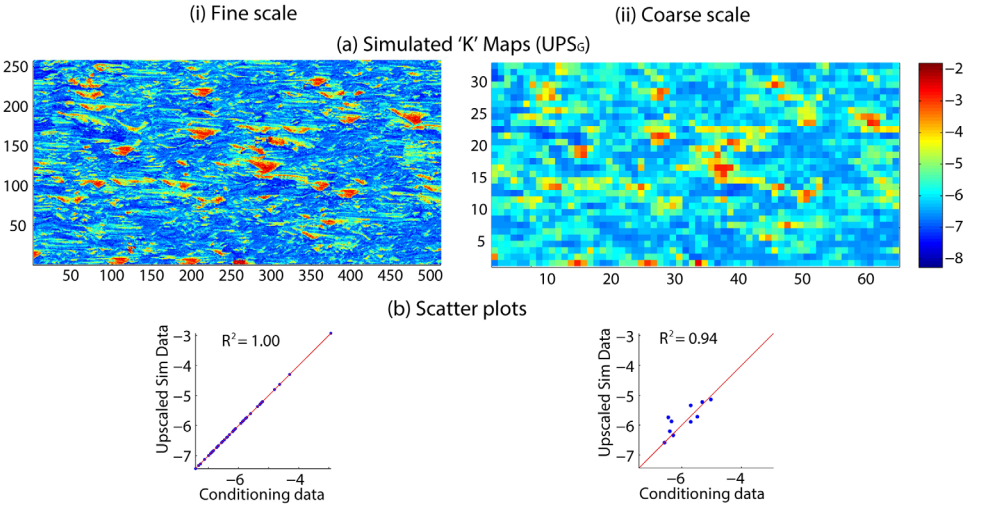

Figure 8. MIQ simulation for a continuous TI with two different scales.

4. Solve the problem with both univariate IQ and MIQ analysis.

5. Validate the MIQ outcome comparing with univariate IQ simulations.

The TI is based on data from a flume experiment simulating sediment deposition in a realistic physical setting [*Paola et al.*, 2009]. Time-lapse images are taken during the experiment, which allow reconstructing the sediment volume. As a result, this is one of the best examples of fully known realistic heterogeneous reservoirs. Our TI consists in one cross section through this volume, and is shown in Figure 7a (left), where the color values have been converted to logarithms of hydraulic conductivity values. We use this example to investigate the use of a large upscaling factor with our method, which reflects situations encountered in real cases. Figure 7a (right) corresponds to a 8X upscaling factor applied to the original fine-scale training image. Conditioning data (Figure 7b) are generated by taking random points from the unconditional realizations shown in Figure 7c, which constitute the reference hydraulic conductivity maps for both scales. We sample 50 and 10 data locations for fine and coarse scale, respectively. The sizes of the TIs and SGs are identical with 256 $\times$ 512 and 32 $\times$ 64 cells for the fine and coarse scales. The same IQ parameters as for the previous example are used to obtain the fine-scale hydraulic conductivity realization.

Before performing multiscale IQ, we start by testing an approach where the scale interactions are ignored. This is done by simulating each scale independently with univariate training images, the fine-scale data being used with the fine-scale TI and the coarse-scale data being used with the coarse TI. The resulting models are shown in Figure 7d. In this case, the conditioning data are honored exactly (Figure 7e), but we know that we are not using all the information at hand since the data at one scale is not used for simulating the other scale. The simulations are then compared to the exhaustively known reference, resulting in a RMSE of 1.41 for the fine scale (Figure 7c, left) and a RMSE of 1.29 for the coarse scale (Figure 7c, left). It is expected that accounting for the interscale relationships should allow better exploiting the available data and therefore obtaining lower RMSE values.

3.2.2. Multiscale MIQ Simulation

We now consider the same example as in Figure 7, but using our methodology to take into account the scale relationships. The same methodology is applied as in the first test case to obtain the fine-scale MIQ realization (Figure 8a, left). Then, we implement the renormalization upscaling technique to produce large-scale conductivity map (Figure 8a, right) using the fine-scale realization. Similarly as in the previous test case, the conditioning data are not exactly matched, as shown in the scatter plots of Figure 8b. The mismatch between the upscaled realization and the coarse data is quite large due to the upscaling factor of 8, i.e., 1 coarse pixel = 64 fine pixels.

For the kriging correction, the variogram adjusted on the fine-scale training image results in following parameters: range = 20, sill = 0.51, and nugget = 0.5. We then perform iterative kriging corrections until all conditioning data are satisfied within a RMSE of 10^{-5}. The simulated hydraulic conductivity maps after

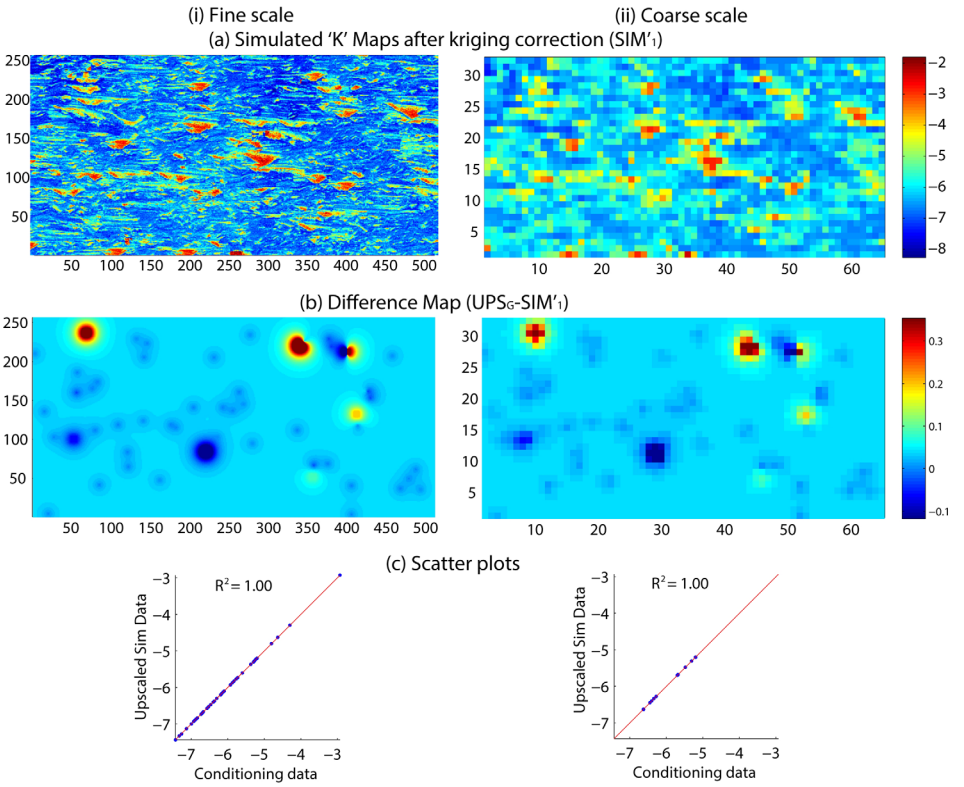

Figure 9. Performance of data conditioning using upscaling with kriging correction for a continuous TI with two different scales. The colorbar in Figure 9a represents logarithm of hydraulic conductivity values, and in Figure 9b, it indicates the differences between both the simulated "K" maps before and after kriging correction.

kriging corrections are shown in Figure 9a, with the difference caused by the kriging correction in Figure 9b. When comparing these realizations with the reference we get RMSE values of 1.28 and 1.04 for fine and coarse scales, which is a significant improvement compared to the case where each scale is considered independently. This indicates that considering the interactions between large and small scales results in an improved characterization of the aquifer.

4. Conclusion

It has been widely demonstrated that the hydraulic conductivity of an aquifer increases with a larger portion of the aquifer tested. This poses a challenge when different hydraulic conductivity measurements coexist in a field study and have to be integrated simultaneously (e.g., core analysis, slug tests and well tests, remote sensing campains). While the scaling of hydraulic conductivity can be analytically derived in multi-Gaussian media, there is no general methodology to simultaneously integrate hydraulic conductivity measurements taken at different scales in highly heterogeneous media. Here we address this issue in the context of MPS simulation.

The key principle of our methodology is to consider the different scales of hydraulic conductivity as joint variables which are simulated together. Based on a TI that represents the fine-scale spatial variability, we use a classical upscaling method to obtain a series of upscaled TIs that correspond to the different scales at which measurements are available. In our case, the renormalization method is used for this upscaling step, but any upscaling method could be employed. Considered together, the different scales obtained are considered a single multiscale representation of the initial TI, in a similar fashion as the multiscale pyramids used in image processing.

We then use IQ, which is a recent MPS simulation method that allows dealing with multivariate TIs, to generate conditional realizations of the different scales together. One characteristic of these realizations is that the possible nonlinear relationships between the simulated scales are statistically similar to the relationships

observed in the multiscale TI. Therefore these relationships are considered a reasonable approximation of the renormalization results that were used on the TI. Another characteristic of these realizations is that they can be directly conditioned to local data, and data at any scale can be considered.

The realizations obtained exactly satisfy the conditioning data across all scales, but it comes at the expense of an approximate representation of the physical scale relationships. In order to mitigate this approximation, we apply a kriging-based correction to the finest scale, which ensures local conditioning at the coarsest scales but may degrade the patterns found in the training image. Significant patterns degradation did not occur in the cases tested. However, if the kriging correction is large compared to the magnitude of the simulated hydraulic conductivity, it can be a symptom that the model setting has to be revisited (i.e., either the structures in the training image are inaccurate, the upscaling scheme is not valid, or the data have measurement errors). The method is tested on a series of synthetic examples with different connectivity properties, where it gives good results and shows potential for the integration of different measurement scales allowing a better characterization of aquifers by making the best possible use of field data.

Acknowledgments
This work was supported by a scholarship from the University of New South Wales and the research projects undertaken as part of the Australian Research Council and National Water Commission funding for the National Centre for Groundwater Research and Training (NCGRT). The data used in this study are available on request to the authors.

References

Abdollahifard, M. J., and K. Faez (2013), Stochastic simulation of patterns using Bayesian pattern modeling, *Comput. Geosci.*, *17*, 99–116.
Allard, D., D. D'Or, and R. Froidevaux (2011), An efficient maximum entropy approach for categorical variable prediction, *Eur. J. Soil Sci.*, *62*(3), 381–393.
Arpat, B., and J. Caers (2007), Conditional simulations with patterns, *Math. Geol.*, *39*(2), 177–203.
Botros, F., A. Hassan, and G. Pohll (2006), Assessment of hydraulic conductivity upscaling techniques and associated uncertainty, paper presented at XVI International Conference on Computational Methods in Water Resources, CMWR, Copenhagen, Denmark.
Boucher, A., and R. Dimitrakopoulos (2012), Multivariate block-support simulation of the Yandi iron ore deposit, Western Australia, *Math. Geosci.*, *44*(4), 449–468.
Boucher, A., C. Kyriakidis, and C. Cronkite-Ratcliff (2008), Geostatistical solutions for super-resolution land cover mapping, *IEEE Trans. Geosci. Remote. Sens.*, *46*(1), 272–283.
Caers, J., S. Strebelle, and K. Payrazyan (2003), Stochastic integration of seismic data and geologic scenarios: A West Africa submarine channel saga, *Leading Edge*, *22*(3), 192–196.
Cardwell, W., and R. Parsons (1945), Average permeabilities of heterogeneous oil sands, *Trans. Am. Inst. Min. Metall. Pet. Eng.*, *160*, 34–42.
Chugunova, T., and L. Hu (2008), Multiple-point simulations constrained by continuous auxiliary data, *Math. Geosci.*, *40*(2), 133–146.
Clauser, C. (1992), Permeability of crystalline rocks, *Eos Trans. AGU*, *73*(21), 233–240.
Comunian, A., S. K. Jha, B. M. S. Giambastiani, G. Mariethoz, and B. F. J. Kelly (2014), Training images from process-imitating methods, *Math. Geosci.*, *46*(2), 241–260, doi:10.1002/2013WR015040.
Dagan, G. (1986), Statistical theory of groundwater flow and transport: Pore to laboratory, 25 laboratory to formation, and formation to regional scale, *Water Resour. Res.*, *22*, 120S–134S.
Dagan, G. (1989), *Flow and Transport in Porous Formations*, Springer, Berlin.
Deutsch, C. V. (2006), A sequential indicator simulation program for categorical variables with point and block data: BlockSIS, *Comput. Geosci.*, *32*(10), 1669–1681.
Dickson, N. E. M., J. C. Comte, J. McKinley, and U. Ofterdinger (2014), Coupling ground and airborne geophysical data with upscaling techniques for regional groundwater modeling of heterogeneous aquifers: Case study of a sedimentary aquifer intruded by volcanic dykes in Northern Ireland, *Water Resour. Res.*, *50*, 7984–8001, doi:10.1002/2014WR015320.
Dijkstra, E. (1959), A note on two problems in connexion with graphs, *Numer. Math.*, *1*, 269–271, doi:10.1007/BF01386390.
Efros, A. A., and W. T. Freeman (2001), Image quilting for texture synthesis and transfer, paper presented at the ACM SIGGRAPH Conference on Computer Graphics.
El Ouassini, A., A. Saucier, D. Marcotte, and B. D. Favis (2008), A patchwork approach to stochastic simulation: A route towards the analysis of morphology in multiphase systems, *Chaos Solitons Fractals*, *36*(2), 418–436.
Emery, X. (2008), Change of support for estimating local block grade distributions, *Math. Geosci.*, *40*(6), 671–688.
Emery, X. (2009), Change-of-support models and computer programs for direct block-support simulation, *Comput. Geosci.*, *35*(10), 2047–2056.
Emery, X., and J. Ortiz (2011), A comparison of random field models beyond bivariate distributions, *Math. Geosci.*, *43*(2), 183–202, doi:10.1007/s11004-010-9305-6.
Emsellem, Y., and G. De Marsily (1971), An automatic solution for the inverse problem, *Water Resour. Res.*, *7*, 1264–1283, doi:10.1029/WR007i005p01264.
Falivene, O., P. Arbués, A. Gardiner, G. Pickup, J. Munõz, and L. Cabrera (2006), Best practice stochastic facies modeling from a channel-fill turbidite sandstone analog (the Quarry outcrop, Eocene Ainsa basin, northeast Spain), *AAPG Bull.*, *90*(7), 1003–1029.
Farmer, C. L. (2002), Upscaling: A review, *Int. J. Numer. Methods Fluids*, *40*(1-2), 63–78, doi:10.1002/fld.267.
Faucher, C., A. Saucier, and D. Marcotte (2012), A new patchwork simulation method with control of the local-mean histogram, *Stochastic Environ. Res. Risk Assess.*, *27*, 253–273.
Gardet, C., M. Le Ravalec, and E. Gloaguen (2014), Multiscale parameterization of petrophysical properties for efficient history-matching, *Math. Geosci.*, *46*(3), 315–336.
Gibson, J. (1950), *The Perception of the Visual World*, Houghton Mifflin, Boston, Mass.
Gomez-Hernandez, J. J., and S. M. Gorelick (1989), Effective groundwater model parameter values: Influence of spatial variability of hydraulic conductivity, leakance, and recharge, *Water Resour. Res.*, *25*, 405–419.
Gomez-Hernandez, J. J., and A. G. Journel (1994), Stochastic characterization of gridblock permeabilities, *SPE Form. Eval.*, *9*(2), 93–99.
Guardiano, F., and M. Srivastava (1993), Multivariate geostatistics: Beyond bivariate moments, in *Geostatistics-Troia*, edited by A. Soares, pp. 133–144, Kluwer Acad., Dordrecht, Netherlands.

Hajizadeh, A., A. Safekordi, and F. A. Farhadpour (2011), A multiple-point statistics algorithm for 3D pore space reconstruction from 2D images, *Adv. Water Resour.*, *34*(10), 1256–1267.
He, X., T. O. Sonnenborg, F. Jørgensen, and K. H. Jensen (2013), The effect of training image and secondary data integration with multiple-point geostatistics in groundwater modeling, *Hydrol. Earth Syst. Sci. Discuss.*, *10*(9), 11,829–11,860, doi:10.5194/hessd-10-11829-2013.
Herzog, B. L., and W. J. Morse (1986), Hydraulic conductivity at a hazardous waste disposal site: Comparison of laboratory and field-determined values, *Waste Manage. Res.*, *4*(2), 177–187.
Hu, L., and T. Chugunova (2008), Multiple-point geostatistics for modeling subsurface heterogeneity: A comprehensive review, *Water Resour. Res.*, *44*, W11413, doi:10.1029/2008WR006993.
Huysmans, M., and A. Dassargues (2012), Modeling the effect of clay drapes on pumping test response in a cross-bedded aquifer using multiple-point geostatistics, *J. Hydrol.*, *450–451*, 159–167.
Jha, S. K., G. Mariethoz, J. P. Evans, and M. F. McCabe (2013), Demonstration of a geostatistical approach to physically consistent downscaling of climate modeling simulations, *Water Resour. Res.*, *49*, 245–259, doi:10.1029/2012WR012602.
Jung, A., D. H. Fenwick, and J. Caers (2013), Training image-based scenario modeling of fractured reservoirs for flow uncertainty quantification, *Comput. Geosci.*, *17*(6), 1015–1031.
Koch, J., X. He, K. H. Jensen, and J. C. Refsgaard (2014), Challenges in conditioning a stochastic geological model of a heterogeneous glacial aquifer to a comprehensive soft data set, *Hydrol. Earth Syst. Sci.*, *18*(8), 2907–2923.
Koltermann, C. E., and S. M. Gorelick (1992), Paleoclimatic signature in terrestrial flood deposits, *Science*, *256*(5065), 1775–1782.
Kupfersberger, H., C. V. Deutsch, and A. G. Journel (1998), Deriving constraints on small-scale variograms due to variograms of large-scale data, *Math. Geol.*, *30*(7), 837–852.
Liu, Y., and A. Journel (2009), A package for geostatistical integration of coarse and fine scale data, *Comput. Geosci.*, *35*(3), 527–547.
Mahmud, K., G. Mariethoz, J. Caers, P. Tahmasebi, and A. Baker (2014), Simulation of Earth textures by conditional image quilting, *Water Resour. Res.*, *50*, 3088–3107, doi:10.1002/2013WR015069.
Marcotte, D. (1994), Direct simulation of block grades, in *Geostatistics for the Next Century*, edited by R. Dimitrakopoulos, pp. 245–258, Kluwer Acad., Dordrecht, Netherlands.
Mariethoz, G., and J. Caers (2014), *Multiple-Point Geostatistics: Stochastic Modeling With Training Images*, 384 pp., Wiley-Blackwell, Oxford, U. K.
Mariethoz, G., and S. Lefebvre (2014), Bridges between multiple-point geostatistics and texture synthesis, *Math. Geosci.*, *66*, 66–80, doi:10.1016/j.cageo.2014.01.001.
Mariethoz, G., M. McCabe, and P. Renard (2012), Multivariate spatio-temporal reconstruction of gaps for spatially continuous satellite based retrievals, *Water Resour. Res.*, *48*, W10507, doi:10.1029/2012WR012115.
Matheron, G. (1967), *Eléments Pour une Théorie des Milieux Poreux*, 168 pp., Masson, Paris.
McHargue, T., M. J. Pyrcz, M. D. Sullivan, J. D. Clark, A. Fildani, B. W. Romans, J. A. Covault, M. Levy, H. W. Posamentier, and N. J. Drinkwater (2011), Architecture of turbidite channel systems on the continental slope: Patterns and predictions, *Mar. Pet. Geol.*, *28*(3), 728–743.
Mustapha, H., and R. Dimitrakopoulos (2011), HOSIM: A high-order stochastic simulation algorithm for generating three-dimensional complex geological patterns, *Comput. Geosci.*, *37*(9), 1242–1253.
Natali, M., T. G. Klausen, and D. Patel (2014), Sketch-based modelling and visualization of geological deposition, *Comput. Geosci.*, *67*, 40–48.
Neuman, S. P. (1990), Universal scaling of hydraulic conductivities and dispersivities in geologic media, *Water Resour. Res.*, *26*, 1749–1758, doi:10.1029/WR026i008p01749.
Okabe, H., and M. Blunt (2007), Pore space reconstruction of vuggy carbonates using microtomography and multiple-point statistics, *Water Resour. Res.*, *43*, W12S02, doi:10.1029/2006WR005680.
Oriani, F., J. Straubhaar, P. Renard, and G. Mariethoz (2014), Simulation of rainfall time series from different climatic regions using the direct sampling technique, *Hydrol. Earth Syst. Sci.*, *18*(8), 3015–3031, doi:10.5194/hess-18-3015-2014.
Paola, C., K. Straub, D. Mohrig, and L. Reinhardt (2009), The "unreasonable effectiveness" of stratigraphic and geomorphic experiments, *Earth Sci. Rev.*, *97*(1-4), 1–43.
Pham, T. D. (2012), Supervised restoration of degraded medical images using multiple-point geostatistics, *Comput. Methods Programs Biomedicine*, *106*(3), 201–209.
Ren, W., C. V. Deutsch, D. Gamer, T. J. Wheeler, J. F. Richy, and E. Mus (2008), Quantifying resources for the surmont lease with 2D mapping and multivariate statistics, *SPE Reservoir Eval. Eng.*, *11*(2), 341–351.
Renard, P., and G. De Marsily (1997), Calculating equivalent permeability: A review, *Adv. Water Resour.*, *20*(5-6), 253–278.
Renard, P., G. Le Loc'h, E. Ledoux, G. de Marsily, and R. Mackay (2000), A fast algorithm for the estimation of the equivalent hydraulic conductivity of heterogeneous media, *Water Resour. Res.*, *36*, 3567–3580.
Rezaee, H., G. Mariethoz, M. Koneshloo, and O. Asghari (2013), Multiple-point geostatistical simulation using the bunch-pasting direct sampling method, *Comput. Geosci.*, *54*, 293–308.
Ronayne, M. J., S. M. Gorelick, and J. Caers (2008), Identifying discrete geologic structures that produce anomalous hydraulic response: An inverse modeling approach, *Water Resour. Res.*, *44*, W08426, doi:10.1029/2007WR006635.
Rovey, C. W., and D. S. Cherkauer (1995), Scale dependency of hydraulic conductivity measurements, *Ground Water*, *33*(5), 769–780, doi:10.1111/j.1745-6584.1995.tb00023.x.
Sanchez-Vila, X., A. Guadagnini, and J. Carrera (2006), Representative hydraulic conductivities in saturated groundwater flow, *Rev. Geophys.*, *44*, RG3002, doi:10.1029/2005RG000169.
Schulze-Makuch, D., and D. Cherkauer (1998), Variations in hydraulic conductivity with scale of measurement during aquifer tests in heterogeneous, porous carbonate rocks, *Hydrogeol. J.*, *6*, 204–215.
Straubhaar, J., P. Renard, G. Mariethoz, R. Froidevaux, and O. Besson (2011), An improved parallel multiple-point algorithm using a list approach, *Math. Geosci.*, *43*(3), 305–328.
Strebelle, S. (2002), Conditional simulation of complex geological structures using multiple-point statistics, *Math. Geol.*, *34*(1), 1–22.
Tahmasebi, P., and M. Sahimi (2013), Cross-correlation function for accurate reconstruction of heterogeneous media, *Phys. Rev. Lett.*, *110*(7), 078002.
Tahmasebi, P., A. Hezarkhani, and M. Sahimi (2012), Multiple-point geostatistical modeling based on the cross-correlation functions, *Comput. Geosci.*, *16*, 779–797, doi:10.1007/s10596-012-9287-1.
Tang, Y., P. M. Atkinson, N. A. Wardrop, and J. Zhang (2013a), Multiple-point geostatistical simulation for post-processing a remotely sensed land cover classification, *Spatial Stat.*, *5*, 69–84.
Tang, Y., P. M. Atkinson, N. A. Wardrop, and J. Zhang (2013b), Multiple-point geostatistical simulation for post-processing a remotely sensed land cover classification, *Spatial Stat.*, *5*, 69–84, doi:10.1016/j.spasta.2013.04.005.

Tran, T. (1996), The 'missing scale' and direct simulation of block effective properties, *J. Hydrol.*, *183*(1–2), 37–56, doi:10.1016/S0022-1694(96)80033-3.

Tsunoyama, T., T. D. Pham, T. Fujita, and T. Sakamoto (2014), Identification of intestinal wall abnormalities and ischemia by modeling spatial uncertainty in computed tomography imaging findings, *Comput. Methods Programs Biomedicine*, *117*(1), 30–39, doi:10.1016/j.cmpb.2014.05.003.

Wu, J., T. Zhang, and A. Journel (2008), Fast FILTERSIM simulation with score-based distance, *Math. Geosci.*, *40*(7), 773–788.

Zhang, T., P. Switzer, and A. Journel (2006), Filter-based classification of training image patterns for spatial simulation, *Math. Geol.*, *38*(1), 63–80.

Zhou, H., L. Li, and J. Jaime Gómez-Hernández (2010), Three-dimensional hydraulic conductivity upscaling in groundwater modeling, *Comput. Geosci.*, *36*(10), 1224–1235, doi:10.1016/j.cageo.2010.03.008.

Zinn, B., and C. Harvey (2003), When good statistical models of aquifer heterogeneity go bad: A comparison of flow, dispersion, and mass transfer in connected and multivariate Gaussian hydraulic conductivity fields, *Water Resour. Res.*, *39*(3), 1051, 10.1029/2001WR001146.